Magnetic gearbox for automotive power transmissions: An innovative industrial technology

(Article begins on next page)

28 April 2024

Contents lists available at ScienceDirect

Engineering Science and Technology, an International Journal

Full length article

Magnetic gearbox for automotive power transmissions: An innovative industrial technology

Luca Dimauro [a],[*], Elvio Bonisoli [a], Mauro Velardocchia [a], Maurizio Repetto [b], Piergiorgio Alotto [c], Mattia Filippini [c], Riccardo Torchio [c]

[a] Department of Mechanical and Aerospace Engineering, Politecnico di Torino, Corso Duca degli Abruzzi 24, 10129, Torino, Italy
[b] Department of Energy "Galileo Ferraris", Politecnico di Torino, Corso Duca degli Abruzzi 24, 10129, Torino, Italy
[c] Department of Industrial Engineering, Universita degli Studi di Padova, Via Gradenigo 6/a, 35131, Padova, Italy

A B S T R A C T

Conventional coaxial magnetic gears are structures with permanent magnets, which working principle is equivalent to that of epicyclic gearing. The motion is transferred between different axles, without contact in the rotating elements, by modulating the magnetic field generated by permanent magnets on inner and outer rotors of the machine, exploiting ferromagnetic poles in the middle rotor. The challenge of replacing standard mechanical gears in an automotive powertrain has led to the development of a new technology of paramount importance for the automotive industry which could solve several problems related to classical gears like, *e.g.* need of lubricant, wearing, vibration, noise, and need of friction material. In this paper a novel topology of magnetic gearbox is proposed. The presented solution is expected to have a higher reliability and efficiency compared to equivalent mechanical gearboxes, allowing the torque transmission from the power source (electrical or thermal) to the wheels, with a certain number of fixed gear ratios. Several topological solutions of magnetic gearbox are proposed, with possible application in different industrial fields. The gearshift phase has been dynamically analysed with an analytical approach and then a magnetic powertrain has been developed in Matlab/Simulink to validate the proposed technology, as alternative to the mechanical one.

1. Introduction

The adoption of magnetic gears (MGs) is propitious since they can transmit motion between rotors without friction [1] or other mechanical contacts. In recent years, the developments and advances in this technology are increasingly leading to the commercial application of MGs and to their implementation in more complicated systems, in substitution of mechanical gears. In the last two decades, different topologies [2] have been proposed to improve performance in terms of torque density. Nowadays, the most common mechanical topologies (external/internal spur gears, worm gears, rack and pinion, etc.) have their magnetic counterparts [3–5]. Recently, also more complex structures have been investigated, as cycloidal MGs [6], combining axial and radial topologies, or conical coaxial magnetic gears [7]. A collection of MGs technologies is proposed in [8], pointing out advantages of this solution with respect to mechanical power transmission in transportation and in wind energy conversion systems.

The coaxial magnetic gear (CMG) is one of the most promising topology [9,10], and basically consist of inner and outer rotors with arrays of permanent magnets (PMs), and of an intermediate rotor made of a number of ferromagnetic pieces, respectively called sun, ring, and carrier. As in mechanical epicyclic gear trains where the number of mechanical teeth define the gear ratio, in the magnetic counterpart the teeth are replaced by the magnetic poles. Different solutions of MGs have been analysed in the literature for hybrid [11] and electric vehicle (EV) [12] applications, to overcome the drawbacks of mechanical gears. By properly varying the speed of the rotors, a magnetic Continuous Variable Transmission (mCVT) can be achieved [13–15], integrating the CMG with a brushless permanent-magnet machine. Consequently, a more compact solution can be realised for EV, in substitution of the mechanical CVT [16]. A bearingless CMG with three-phase windings is proposed in [17] to provide, besides torque transmission, additional magnetic levitation capabilities, also investigated in [18]. In recent years, several researchers faced the topic of MGs optimisation as proposed in [19], where a genetic algorithm (GA) is combined with Taguchi method to evaluate the influence of each parameter in MGs, or as done by others which proposed a structure with a double-layer of PMs [20], or a novel dual-flux modulator [21], aiming at increasing
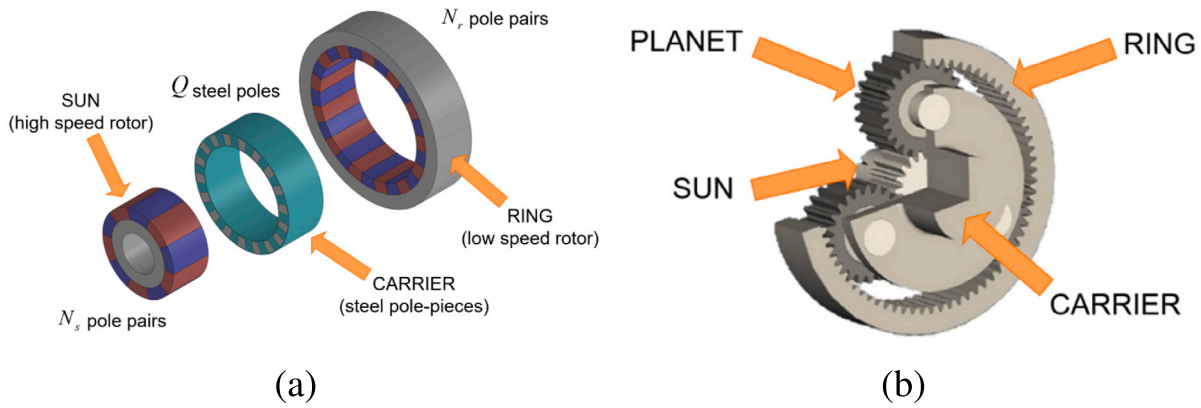

Fig. 1. Rotors of a coaxial magnetic gear (a) and elements of a mechanical planetary gear train (b).

the torque density, meanwhile reducing the cogging torque [22] and the iron losses [23].

The possible implementation of magnetic gearbox technology to automotive applications can lead to higher transmission efficiencies if compared to the mechanical counterpart [24]. The authors have already worked on the topic of MGs, regarding their optimisation [25] and the analysis of magnetic losses [26], and are now developing the magnetic gearbox technology [27] with funded research projects, achieving interesting preliminary results [28,29]. By controlling the motion of the three rotors of a CMG a speed differential can be implemented in the transmission driveline as it is patented in [30].

The paper is organised as follows: Section 2 proposes an analysis of similarities and differences between CMG and mechanical planetary gears, Section 3 introduces the concept of magnetic gearbox and its role in the automotive drivetrain. In Section 4, all the patented solutions of the magnetic gearbox technology are proposed as different topological arrangements. Then, in Section 5, the gearshift procedure is firstly analysed from an analytical point of view and then studied using a Simulink model of the transmission driveline. Finally, in Section 6, some details and comments concerning the manufacturing of the magnetic gearbox prototype are provided.

2. Similarities and differences between coaxial magnetic gears and mechanical planetary gears

Since the CMG presents an analogy with the equivalent mechanical device, its main three rotors, illustrated in Fig. 1(a), are named in the same way: the *sun* is the inner magnetic rotor, the *ring* is the outer one, while the modulating element, holding the ferromagnetic iron poles, is called *carrier*. Several possible kinematic combinations are available, by properly fixing some elements. Two possible arrangement are available for both CMG and mechanical planetary gears: in the first one, the device works as an ordinary gear train, hence the positions of the rotor axes in the space during their rotation are always the same, while in the second one, under certain working conditions, the device acts as a planetary gearbox and planet axes assume a different spatial position. Planetary gear trains are often adopted in case of certain limitations in terms of space and weight, since with these devices larger speed reduction and higher power density can be achieved in a small volume, with respect to ordinary gear trains or external spur gears.

The angular rotational speeds ω_s, ω_c and ω_r of sun, carrier, and ring, respectively, are related by means of kinematic relationship which can be evaluated using the carrier as the centre of a global reference system. When the CMG is considered as an ordinary magnetic gearing, the carrier is kept fixed, *i.e.* $\omega_c = 0$, and the transmission ratio between sun and ring can be evaluated using the Willis equation [31], which is

written for both magnetic and mechanical solutions:

$$\begin{cases} \tau_{s,r_{magn}} = \dfrac{\omega_s - \omega_c}{\omega_r - \omega_c} = \dfrac{\omega_s}{\omega_r} = -\dfrac{N_r}{N_s} < 0 \\ \tau_{s,r_{mech}} = \dfrac{\omega_s - \omega_c}{\omega_r - \omega_c} = \dfrac{\omega_s}{\omega_r} = -\dfrac{Z_p}{Z_s} \cdot \dfrac{Z_r}{Z_p} = -\dfrac{Z_r}{Z_s} < 0 \end{cases} \quad (1)$$

where N_s and N_r are the number of PM pole pairs at sun (internal) and ring (external) rotors in the magnetic solution, while Z_s, Z_p, and Z_r are the number of teeth of sun, planets, and ring gears, respectively, in a mechanical planetary gear train. If the ring rotor is kept fixed instead, *i.e.* $\omega_r = 0$, the transmission ratio between sun and carrier is given by Eq. (2):

$$\begin{cases} \tau_{s,c_{magn}} = \dfrac{\omega_s}{\omega_c} = \dfrac{N_s + N_r}{N_s} = 1 + \dfrac{N_r}{N_s} = 1 - \tau_{s,r_{magn}} = 1 + \left| \tau_{s,r_{magn}} \right| > 0 \\ \tau_{s,c_{mech}} = \dfrac{\omega_s}{\omega_c} = \dfrac{Z_s + Z_r}{Z_s} = 1 + \dfrac{Z_r}{Z_s} = 1 - \tau_{s,r_{mech}} = 1 + \left| \tau_{s,r_{mech}} \right| > 0 \end{cases} \quad (2)$$

Therefore, in the first case an inversion or motion between input (sun) and output (ring) is realised, while in the second one the rotational speeds of sun and carrier rotors have the same sign. Assuming Q as the number of carrier ferromagnetic poles, for a given CMG geometry, only particular triplets (N_s, N_r, Q) lead to steady state torque transmission between input and output, where the combination $Q = N_s + N_r$ gives the highest transmissible torque. Instead, in the equivalent mechanical device the relationship $Z_r = Z_s + 2Z_p$ must be respected, since the number of teeth is correlated to the radius of gears r by the module parameter $m = \dfrac{2r}{Z}$. Both the relationships correlate the geometrical and constructive parameters of gears and rotors, but with a strong difference, if the carrier is kept fixed:

- the CMG can operate both as a speed reducer and as a speed multiplier when the input power is connected to the sun and the output to the ring. This assumption depends on the number of PM on inner and outer rotors, hence the two operating conditions are ensured when $N_s < N_r$ and with $N_s > N_r$, respectively;
- in a mechanical planetary gear train the rotational speed of ring will be always lower than the sun speed, since the geometrical and constructive relationship $Z_r = Z_s + 2Z_p > Z_s$ must be respected [31], hence to have a speed multiplier it is necessary to switch input/output.

Moreover, in mechanical planetary gear train, for the same torque T to be transmitted, the higher the number of planets N_p, the lower the force F acting on the teeth of the planetary gears, since relation $F = \dfrac{T}{r_p N_p}$ must be respected; this allows to use planets with a much smaller radius r_p, to have a more compact speed reducer. A further benefit is the possibility of withstanding high radial loads on the shaft, since the forces transmitted between the gears are mutually balanced [24]: their resultant is zero, hence only the torque transmitted by the gearbox must be balanced by gearbox bearings. On the other side, for the magnetic

solutions, planets are virtual, hence the magnetic field generated by PMs of the two rotors is modulated by the array of ferromagnetic poles.

Another important difference between the two solutions relies on the meshing stiffness. Mechanical gear wheels have a meshing stiffness much higher than transmission torsional stiffness, while a magnetic transmission, due to the absence of a direct contact, is inherently elastic, hence its coupling stiffness is comparable with transmission stiffness. Thereby, it is necessary to act on the controller to avoid speed/torque oscillations [32] and to avoid losing of synchronism between rotors.

According to Eq. (1), a mechanical planetary gear train has 2 Degrees of Freedom (DoFs), hence to evaluate the angular velocity of one rotor, *e.g.* the ring, it is necessary to know the rotational speeds of the other two elements (sun and carrier). Similarly, in CMG, which are synchronous machines, the ring speed ω_r in steady-state conditions is defined once ω_s and ω_c are fixed; this means that in steady state operation slip cannot occur, even if the transmission is contactless. The ring rotational speed ω_r can be computed using Eq. (3) for magnetic and mechanical solutions:

$$\begin{cases} \omega_r = -\frac{N_s}{N_r}\omega_s + \left(1 + \frac{N_s}{N_r}\right)\omega_c = -\frac{N_s}{Q-N_s}\omega_s + \frac{Q}{Q-N_s}\omega_c \\ \omega_r = -\frac{Z_s}{Z_r}\omega_s + \left(1 + \frac{Z_s}{Z_r}\right)\omega_c = -\frac{Z_s}{2Z_p+Z_s}\omega_s + \frac{2(Z_p+Z_s)}{(2Z_p+Z_s)}\omega_c \end{cases} \quad (3)$$

Planetary gear trains are largely used in applications where high transmission ratio must be realised, with a consequently high torque increment, or when the power, coming from three different axes, must be connected, as it happens for an automotive differential or in a parallel–series hybrid transmission [33,34] where a mechanical Power Split Device (PSD) is used to optimal manage the power flow, generated by the different power sources. The power system indeed comprises two electric motors, *i.e.* MG1 (which during regenerative braking acts as generator), MG2 and the Internal Combustion Engine (ICE). In full-electric mode, only motor MG2 generates power up to a certain medium level, while the ICE and MG2 are used in a hybrid mode when the maximum power is needed at wheel axes, as dynamically analysed in [35] using an electrically variable transmission (EVT) for HEVs. Appropriate control strategies may be developed to improve the transmission efficiency [36] and the transition between the energy sources [37].

3. Magnetic gearbox description

Starting from the concept and working principle of a CMG, the magnetic gearbox technology [27] can be achieved, just collecting several magnetic gears, as potential solution to substitute a multi-stage mechanical gearbox [38]. Thus, an assembled structure with a common translating element, *i.e.* the carrier, is realised. According to the desired transmission ratio, the carrier axially moves to modulate the magnetic field between inner and outer rotors of the gearbox through its ferromagnetic poles. Due to the high performance required by operative conditions, it is mandatory to design new components by means of the most accurate and robust possible techniques based on a multi-physical approach. Simulation methods and procedures are still available but the innovative nature of the recently patented device requires an appropriate tuning and validation. The authors have designed and manufactured a magnetic gearbox prototype, which in their knowledge has not been discussed in literature yet, to validate the patented idea, assessing meanwhile its possible implementation in an automotive driveline. Hence, a test bench for power transmission application has been realised, with limited torque values at low-speed side, as usually done for laboratory applications, and a transmitted torque density of ~ 50 kNm/m^3 for the two gear. Moreover, the test rig is used for the experimental validation of the performance of MG technology, as previously done in [10,39–43].

In automotive applications, the gearbox is an essential component for the power transmission and typically consists of mechanical gears
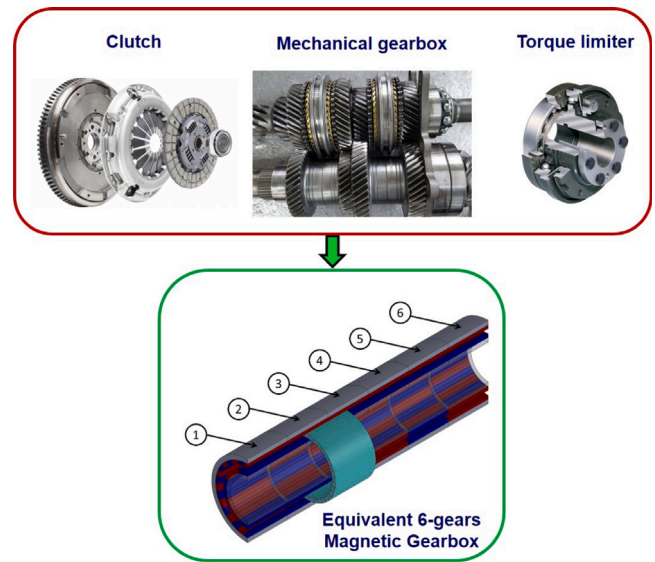

Fig. 2. Driveline complexity reduction using a magnetic gearbox.

requiring the use of a clutch to decouple the rotating elements during gearshifts. Similarly, the differential is fundamental when the vehicle turns, allowing, *e.g.*, the outer drive wheel to spin faster than the inner drive wheel, to accommodate the different radii of turns travelled by the different wheels. In this context, the magnetic transmission (and more generally the MGs) represent a potential alternative to mechanical transmissions, that may overcome several well-known issues, related to Noise Vibration Harshness (NVH) performance [44,45], such as noise and vibration phenomena, which can be linked to mechanical contacts inside transmission driveline [46,47], or addressed to the clutch [48] or to engine torque fluctuations [49], or to the wheels [50,51]. On the other side, some researches faced the topic of vibration in MGs due to electromagnetic force [52,53], performing a signature for the evaluation of acoustic noise and vibrations due to cogging torque and unbalanced radial magnetic forces [54] or proposing bamper bars to reduce torque oscillations [55]. Besides these advantages, the magnetic differential technology [56] makes it also possible to easily introduce advanced safety and driving pleasure enhancement strategies, including torque vectoring [57,58].

The proposed magnetic gearbox technology enables the integration of clutch and torque limiter functions inside the gearbox itself, as conceptually illustrated in Fig. 2, while avoiding the implementation of other mechanical components, typically used in the automotive driveline and which are affected by wear. Operation as clutch occurs thanks to the possibility of varying the transmission ratio without physically disengaging the engine from the gearbox, while the torque limiter function comes into play when a torque, higher than the maximum transmissible torque, is applied to the gearbox, leading to slip between the rotors and avoiding damages as it can be happen in mechanical gears. Moreover, the adoption of MGs in the transmission solves the problem of gear engagement noise, since the torque transfer between input and output takes place without contact between the components, ensuring an automatic overload protection. Finally, the lack of contact between the components avoids the need for lubricants, ensuring a longer life to the system and an environmental benefit with the reduction of polluting materials and dusts.

4. Patented solutions and their application

The magnetic gearbox invention can potentially be used in several industrial sectors. The automotive field is certainly the closest for the development and marketing of the proposed technology, with its
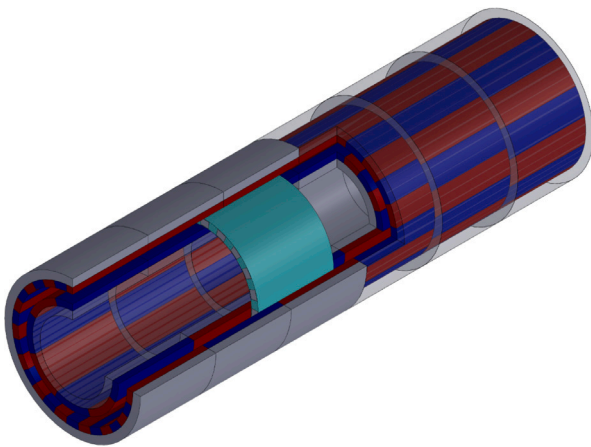
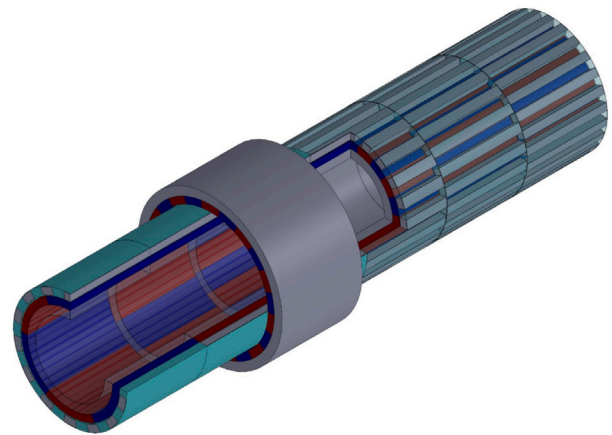**Fig. 3.** Magnetic gearbox solution with a moving carrier.

Fig. 4. Magnetic gearbox solution with moving ring.

possible implementation in traditional vehicles with internal combustion engines, in hybrid vehicles, and in innovative fully EVs. The aforementioned technology may strongly affect other industrial sectors as automation and robotics, aerospace, military, and wind energy. In the automotive field, gearbox systems are used to properly vary the torque transferred from the engine to the vehicle wheels through a transmission driveline. Similarly, gearbox systems are notoriously used in other different industrial fields as, *e.g.*, in electrical tools, in surgical instruments, and in energy converters by means of wind turbines, or other devices, where high speed values can be reached with this innovative technology. Multiple topological variations of magnetic gearboxes have been proposed by the authors in the patent [27], to replace, with several advantages, a conventional mechanical gearbox in all the application fields where it is necessary to vary the transmission ratio between the output of a mechanical power source and the input of a generic user device, hence modulating the transmitted power as a product of torque and rotation speed. Only the arrangements of the magnetic part composing the magnetic gearbox are here presented. Also the mechanical structure, including bearings and plates, should be designed, to guarantee the coaxiality of the rotating parts of the gearbox and the possibility of properly fix some elements, depending on the desired input/output power connections.

4.1. Magnetic gearbox with translating carrier

In the first topological solution, the carrier is subjected to an axial displacement in order to engage with the appropriate gear to transmit torque between input and output at a specific transmission ratio. This solution is reported in Fig. 3, where a possible configuration with six transmission ratios is chosen, adapting the magnetic gearbox to an automotive use. The presence of the moving carrier implies that the number of ferromagnetic poles is constant, and thus the number of PMs pole pairs on inner and outer rotors should properly change for each gear to respect one of the fundamental equations of magnetic gears, namely that the number of ferromagnetic poles Q must be equal to the sum of inner N_s and outer rotors N_r PM pole pairs. For sake of clarity $Q = N_s^{ID} + N_r^{ID}$, where the ID corresponds to the number which identify the transmission ratio. In the proposed arrangement, the neutral position has not been considered, yet. In the same figure it is possible to notice how the carrier moves axially inside the magnetic gearbox, engaging with the third gear, with the assumption that the first gear is on the left and the sixth on the right part of the figure.

The transition phase between the disengagement of the off-going gear and the engagement of the on-coming gear requires to understand what are the effects on speed and torque transmitted between inner and

outer rotors and the required time to synchronise the two rotors according to the new transmission ratio of the magnetic gearbox, depending on the number of PM pole pairs of the magnetic gear the is going to be used. As already mentioned, the use of the clutch can be avoided with the proposed invention of magnetic gearbox, although it is an essential component in a mechanical gearbox. In fact, by means of an adequate control of the input motor speed, during the new gear engagement, the carrier is moved without any interruption of the motion transmission between the involved rotors, *i.e.* the sun connected to the input and the ring connected to the output. Moreover, unlike what happens in the mechanical counterpart, the translation of the carrier is not hindered by the presence of constraints deriving from the axial and rotational mechanical contact between the rotating elements of the synchroniser, that is the key component of a mechanical gearbox.

4.2. Magnetic gearbox with translating ring

A further possible solution for the magnetic gearbox technology consists in having the outer rotor, namely the ring, as the common element of the gearbox, instead of the intermediate rotor, namely the carrier. This solution is represented in Fig. 4. According to this second configuration, the number of PM pole pairs for the common outer rotor remains constant while, unlike the previous configuration, the number of ferromagnetic poles of the carrier varies, to fulfil the equation on the proper number of PMs and ferromagnetic poles. On the other side, the number of PM pole pairs on the inner rotor is instead different for each of the single magnetic gears that make up the magnetic gearbox, according to the relationship $Q^{ID} = N_s^{ID} + N_r$, where the ID corresponds to the number which identify the chosen transmission ratio. This configuration is particularly advantageous from an economic point of view, since the costs related to the construction of the permanent magnets on the outer rotor is significantly reduced. According to this solution, a possible arrangement could be with the power source connected to the inner rotor, while the output shaft can be connected either to the external ring or to the intermediate rotor. In the first case, the outer rotor will be subjected to a roto-translation, especially during the gear engagement, rotating in opposite direction with respect to the inner rotor, while the ferromagnetic rotor has only the function of concatenating the magnetic flux between PMs of inner and outer rotors. Instead, as regards the second case, the outer rotor will be devoted only to the axial translation, while the intermediate rotor will be connected to the output, rotating in the same direction of the input shaft.
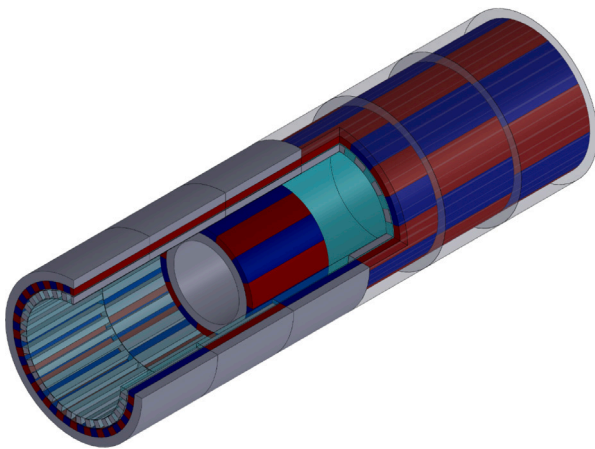
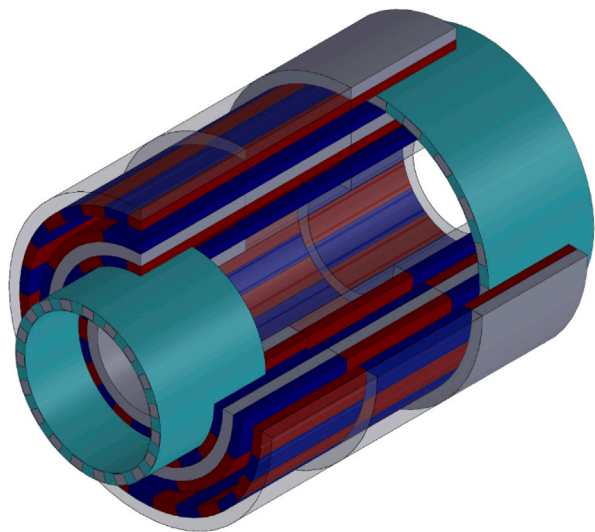**Fig. 5.** Magnetic gearbox solution with moving sun.

Fig. 6. Multi-stage magnetic gearbox solution with two moving carriers.

4.3. Magnetic gearbox with translating sun

Another innovative solution for a magnetic gearbox, in contrast with the previous one, consists in having the inner rotor, namely the sun, as the common element of the magnetic gearbox. The proposed solution is reported in Fig. 5. According to this third possible configuration, the number of PM pole pairs for the common inner rotor remains constant while the number of ferromagnetic poles of the carrier and of the PMs on the outer rotor varies to fulfil the equation $Q^{ID} = N_s + N_r^{ID}$. For this solution, as for the previous one, two possible arrangements could be proposed: in the former the inner rotor will be subjected to a roto-translation, especially during the gear engagement, while in the latter it is devoted only to the axial translation. To be clear, different combinations of input/output can be arranged with the three rotors, to ensure the desired transmission ratio and the desired rotation direction for the shafts of the magnetic gearbox.

4.4. Two-stage magnetic gearbox with two translating carriers

A more compact innovative solution can be achieved with a multi-stage magnetic gearbox, based on the concept of a triple-speed CMG, proposed in [59] for wind turbine application. The axial length of this solution is lower with respect to the previously presented architectures, although an higher complexity of the structure, in radial direction is

necessary. In the meantime, however, the complementary mechanical structure, to allow the coaxiality of rotors and the translation of the two carriers, increases the final product dimensions. In Fig. 6, a two-stage magnetic gearbox is reported. It is made of three rotors, namely inner, middle, and outer rotors and two moving carriers, which are necessary for the magnetic interaction between other rotating elements. In this new arrangement, the relation $Q = N_s + N_r$ holds for both coupling between inner and middle rotor through the inner carrier and interaction between middle and outer rotor by means of the external carrier. This proposed solution can be used in two different ways. In the former, the two stages are used to amplify the transmission gear ratio of the single stage, so it is possible to combine the axial positions of the two carriers to achieve several different transmission ratios, which number depends on the stage number and on the number of magnetic gears for the single stage. Hence, assuming for this case a stage number of $N_{stage} = 2$ and setting the number of magnetic gears equals to $N_{MG} = 3$, the total number of transmission gear ratios is $N_{tau} = N_{MG}^{N_{stage}}$. Instead, in the latter operating condition, and in similarity with the Dual Clutch Transmission (DCT) proposed in [46], the power input can be connected to the middle rotor, while the inner and outer rotors can be considered as the two secondary shafts of a DCT transmission. Therefore, for a six-gears gearbox, the outer rotor can be used for the first three gears, namely from 1st to 3rd, which require a higher torque than the input shaft, since the torque capability of a magnetic gear depends on some geometrical parameters and in particular it is proportional to L and D^2, where L is the axial length and D is the diameter. On the other side, the inner rotor is used for the gears from 4th to 6th, which require a lower torque and higher rotational speeds than the input shaft.

5. Analysis of gearshift procedure

The dynamic analysis of the transition phase during the gear engagement in a magnetic gearbox is an essential step for the appropriate control of the associated test-bench, used for power transmission application. Several control strategies have been proposed in the literature for automated manual transmission (AMT) in EVs through the development of a model in Matlab/Simulink and in Adams [60], which considers stiffness, damping and possible nonlinear contacts, due to backlash, in the gear mesh and inside the synchroniser, or to improve the shift quality of a DCT [61], in terms of speed gradient of the input shaft.

5.1. Analytical approach for gearshift

First, a simple dynamic model, representing a motor connected to the vehicle load through a magnetic gearbox is considered. Then, five different manoeuvres are considered to switch from the first gear ratio to the second one, including two acceleration phases to achieve the stationary condition at a certain gear ratio and three phases to manage the upshift phase. In a transmission driveline the study and analysis of the dynamic behaviour of its inner components is necessary to understand the system response during upshifts or downshifts. In this section, an analytical approach is used to study the transition phase, integrating the differential equations, or solving them with the Matlab function ode45.

The transmission driveline analysed is illustrated in Fig. 7(a), where at one side an electric motor is connected to the sun rotor of the magnetic gearbox, while on the other side a load, modelled as a rotating inertia, represents the vehicle resistance and it is connected to the carrier of the magnetic gearbox. The ring of gearbox is kept fixed. Moreover, the inertias of sun and carrier are included in the inertias of motor and load, hence the 2 DoFs of the transmission are the rotation of motor and the rotation of the load. The differential equation of the transition phase can be written starting from the Free Body Diagrams (FBDs) of the driveline components, as done in Fig. 7(b). According
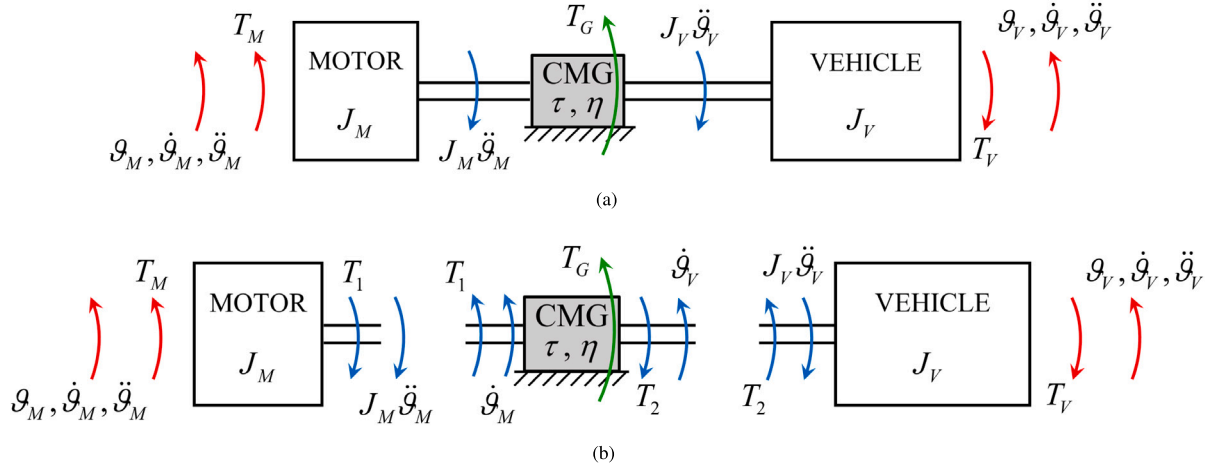
Fig. 7. Schematic diagram of simplified transmission driveline (a) and FBDs of its components: motor, gearbox, and vehicle load.

to Fig. 7, the subscripts M, V, 1 and 2 are related to the motor, to the vehicle, and to the inner dynamics between motor and CMG or between CMG and vehicle, respectively. Finally, the differential equations of transmission model with 2 DoFs are reduced to the equation of an equivalent system with only one DoF, represented by the rotation of motor.

The CMG engaged in the magnetic gearbox is characterised by a given gear ratio τ and by an efficiency η. For the first subsystem, *i.e.*, the motor, its dynamic equation is written as:

$$T_M - T_1 - J_M \frac{d\dot{\theta}_M}{dt} = 0 \qquad (4)$$

where T_M and T_1 are the motor torque and the load torque given by CMG, respectively, while J_M in the motor moment of inertia. Instead, for the second subsystem, *i.e.*, the CMG, Eq. (5) can be written:

$$\eta = \frac{P_{out}}{P_{in}} = \frac{T_2}{T_1} \frac{\dot{\theta}_V}{\dot{\theta}_M} = \frac{T_2}{T_1} \frac{1}{\tau} \qquad (5)$$

where $\tau = \frac{\dot{\theta}_M}{\dot{\theta}_V}$ is the gear ratio between input and output rotational speeds. The torque $T_G = T_2 - T_1$ corresponds to the torque supported by gearbox constraints. The power source is assumed to be connected to the sun of the CMG, while the output is connected to the carrier. The ring rotation is blocked, hence it can only translate for the gear engagement, as shown in Fig. 9. For the third subsystem, which represents the vehicle load, Eq. (6) is written:

$$T_2 - T_V - J_V \frac{d\dot{\theta}_V}{dt} = 0 \qquad (6)$$

where T_R and T_2 are the resistant torque and the internal torque between load and CMG, respectively, while J_V in the moment of inertia that represents the vehicle. It is now possible to write the dynamic equation of an equivalent system, where rotational acceleration and speeds are evaluated at the input motor as well as resistant torque and moments of inertia. The characteristic equation of the equivalent system is here reported:

$$T_M - \tilde{T}_V - J_{eq} \frac{d\dot{\theta}_M}{dt} = 0 \qquad (7)$$

where $\tilde{T}_V$ is the resistant torque evaluated at the input motor and $J_{eq} = J_M + \frac{J_V}{\eta \tau^2}$ is the equivalent moment of inertia of the global system. Differential is not considered in this simplified driveline, hence the vehicle load reduced to the motor results much higher than it really is, causing a slowly dynamics of the driveline. As previously mentioned, the analysed magnetic gearbox consists of two different CMG with a different gear ratio. The torque profile for the input motor, that depends on its rotational speed, and two different resistant torques, one for each
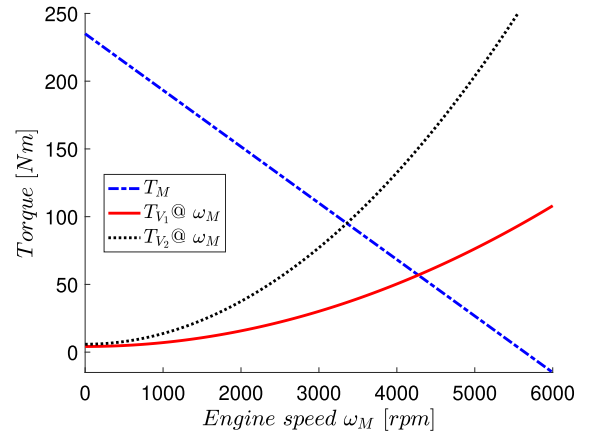

Fig. 8. Operative torque characteristic of a magnetic gearbox driveline.

gear ratio τ, are reported in Fig. 8. The motor torque law is given by Eq. (8):

$$T_M = T_{M_0} - k_M \dot{\theta}_M - T_{B_M} \qquad (8)$$

where k_M is a constant related to the slope of the dash-dotted blue line in Fig. 8, which represents a simplified linear torque characteristic for an electric motor, T_{M_0} is the maximum torque at null engine speed, while T_{B_M} are the dissipative torques related to the vehicle utilities and to the bearings on the first part of the driveline [62]. A simplified direct current (DC) motor characteristic is chosen, to easily manage with the differential equations, instead of using the well-known characteristic of a internal permanent magnet (IPM) motor. The two vehicle resistant torques (red and black lines) are instead related to the vehicle rolling resistance and it could be written as Eq. (9):

$$T_V = f_0 + f_2 \dot{\theta}_V^2 + T_{B_V} \qquad (9)$$

where f_0 and $f_2 = 0.5 \rho C_d A_f R^3$ are two constant terms depending on wheel radius R, tyre parameters, and vehicle dimensions, *e.g.* air density ρ, drag coefficient C_d, vehicle frontal area A_f [63], while T_{B_V} represents the dissipative torque related to the bearings on the second part of the transmission driveline.

The vehicle resistant torques are evaluated using the input motor rotational speed. In Fig. 8, the intersection of the blue line with the two resistant torques returns the stationary condition for both the transmission gear ratios. In Table 1, reasonable values for the system

Table 1
Adopted parameters for the magnetic transmission.

Type	Parameter	Value
Inertia	J_M	0.025 kg m^2
	J_V	130 kg m^2
Bearing torque	T_{B_M}	3 Nm
	T_{B_V}	4 Nm
Rolling resistance	f_0	10 Nm
	f_2	0.0123 Nm s^2/ rad^2
Transmission gear ratio	τ_1	18/5 = 3.6
	τ_2	18/7 = 2.57
Motor	k_M	0.398 Nm/rad
Gearshift time	t_{GS}	1 s
	t_N	0.193 s

parameters are listed: t_{GS} corresponds to the total time for disengagement and engagement, while t_N is the time in neutral position. The equivalent vehicle inertia J_V is computed as $J_V = M R^2$, where R is the wheel radius and M is the mass of vehicle. The simulated manoeuvre, including the gearshift, counts five different phases:

- vehicle acceleration with the first gear ratio τ_1;
- disengaging;
- neutral condition (input/output shafts are decoupled);
- engaging;
- vehicle acceleration with the second gear ratio τ_2.

The first acceleration phase is governed by Eq. (10):

$$\frac{d\dot{\theta}_M}{dt} = \frac{T_M - \tilde{T}_V}{J_{eq}} = \frac{\left(T_{M_0} - k_M\dot{\theta}_M - T_{B_M}\right) - \left(\frac{f_0}{\tau_1\eta} + \frac{f_2}{\tau_1{}^3\eta}\dot{\theta}_M^2 + \frac{T_{B_V}}{\tau_1\eta}\right)}{J_{eq}}$$

(10)

where $\tilde{T}_V = \frac{T_V}{\tau\eta}$ is the equivalent torque of the load reduced to the motor, with τ depending on the gear ratio of the gear considered. This phase allows the system to get the first stationary condition. After that, the disengaging phase occurs. The input motor torque is linearly reduced, according to Eq. (11), and the system is in a configuration like the one reported in Fig. 9(a).

$$T_{M,2} = T_M \left(1 - x_{GS}\right) = T_M \left[1 - \frac{2\left(t - t_1\right)}{t_{GS}}\right]$$

(11)

where $T_{M,2}$ is the input torque in the second phase, $0 \leq x_{GS} \leq 1$ is the axial displacement of the ring inside the magnetic gearbox from the engaged position ($x_{GS} = 0$) to the neutral one ($x_{GS} = 1$). Then, t_{GS} is the total time for disengaging and engaging, and t_1 is the time at the end of the first acceleration phase. A linear partialization of the input torque is assumed when the external ring is translating, since only a part of the magnetic field generated by outer rotor is modulated by the ferromagnetic poles. For sake of clarity, the length of neutral condition is assumed equal to the lengths of the two magnetic gears. The disengaging phase is governed by the differential equation reported in Eq. (12), which is valid up to the complete disengagement happening at t_2:

$$\frac{d\dot{\theta}_M}{dt} = \frac{\left[\left(T_{M_0} - k_M\dot{\theta}_M\right)\left(1 - \frac{2(t-t_1)}{t_{GS}}\right) - T_{B_M}\right] - \left(\frac{f_0}{\tau_1\eta} + \frac{f_2}{\tau_1{}^3\eta}\dot{\theta}_M^2 + \frac{T_{B_V}}{\tau_1\eta}\right)}{J_{eq}}$$

(12)

In the third phase, the input motor and the vehicle load are uncoupled, as in Fig. 9(b), in order to suddenly reduce motor speed to correctly complete the engaging phase. The governing equations
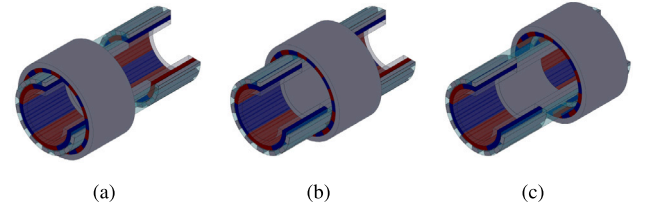

Fig. 9. Magnetic gearbox during disengaging (a), in neutral position (b), and engaging (c).

(Eq. (13)) are:

$$\begin{cases} \frac{d\dot{\theta}_M}{dt} = -\frac{T_{B_M}}{J_M} \\ \frac{d\dot{\theta}_R}{dt} = -\frac{f_0 + f_2\dot{\theta}_R^2 + T_{B_V}}{J_R} \end{cases}$$

(13)

This phase continues until time t_3 when $\dot{\theta}_M = \tau_2\dot{\theta}_R$, then the engaging phase begins, as illustrated in Fig. 9(c), followed by another acceleration phase. During the engaging phase the system governing equation is reported in Eq. (14)

$$\frac{d\dot{\theta}_M}{dt} = \frac{\left[\left(T_{M_0} - k_M\dot{\theta}_M\right)\left(\frac{2(t-t_3)}{t_{GS}}\right) - T_{B_M}\right] - \left(\frac{f_0}{\tau_2\eta} + \frac{f_2}{\tau_2{}^3\eta}\dot{\theta}_M^2 + \frac{T_{B_V}}{\tau_2\eta}\right)}{J_{eq}}$$

(14)

Finally, in the last acceleration phase the system equation is the same of Eq. (10), but using τ_2 instead of τ_1. Hence, Eq. (15) can be written:

$$\frac{d\dot{\theta}_M}{dt} = \frac{T_M - \tilde{T}_V}{J_{eq}} = \frac{\left(T_{M_0} - k_M\dot{\theta}_M - T_{B_M}\right) - \left(\frac{f_0}{\tau_2\eta} + \frac{f_2}{\tau_2{}^3\eta}\dot{\theta}_M^2 + \frac{T_{B_V}}{\tau_2\eta}\right)}{J_{eq}}$$

(15)

The rotational speeds of the input motor and of the output shaft are reported in Fig. 10. The four dashed vertical black lines separate the five different phases of the upshift manoeuvre.

The time in neutral position t_N, at $t_2 \leq t \leq t_3$, is necessary to decrease the engine speed up to the new rotational speed, determined by the new transmission gear ratio τ_2. To conclude, the trend of the input motor torque is reported during the analysed upshift phases. During the disengaging and the new engaging phase, a linear decrement of the transmitted torque is assumed by the authors. Hence, in these conditions the CMG transmit only a portion of its maximum transmissible torque, depending on the axial translation law of the axially translating element, as represented by the $T_{M,2}$ and $T_{M,4}$ in Fig. 11(b).

5.2. Dynamic design of a CMG

Before analysing the Simulink dynamic model of a magnetic gearbox, it is necessary to describe the dynamic equations of a coaxial magnetic gear, which are in analogy with the equations of a mechanical planetary gear train, as previously described for the kinematic relationships. In the magnetic solution, the torque transmission is realised by means of a magnetic contactless stiffness, instead of a contact stiffness, ensuring a contactless torque transmission between the rotating parts. The free body diagram (FBD) of a CMG, composed of sun, ring, and carrier rotors, is reported in Fig. 12. The angular velocities of sun, ring, and carrier and corresponding torques are assumed with same direction. Concordance in their signs corresponds to the input power of the system, while discordance corresponds to output power. The equations of motion of the 3 DOFs of the PMG are defined starting from the free body diagrams of sun, carrier, and ring, which are analysed in Fig. 13.
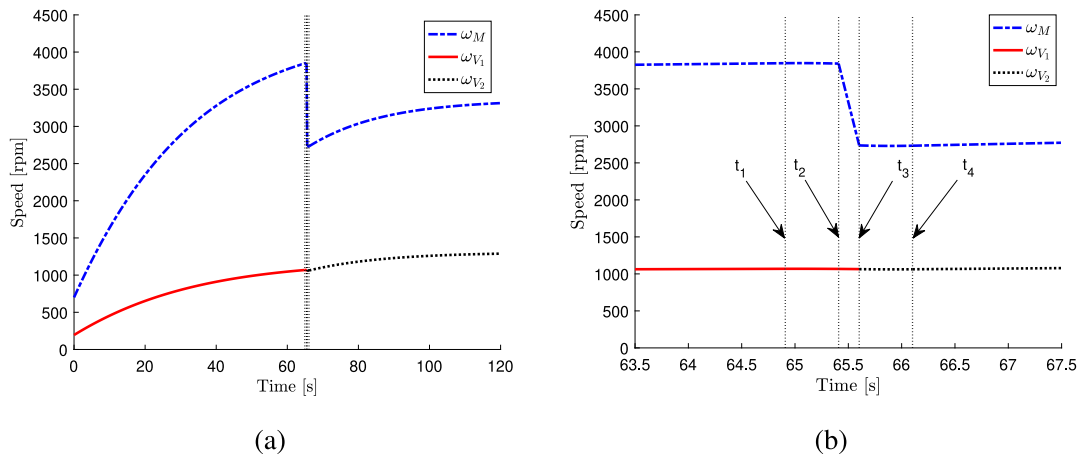
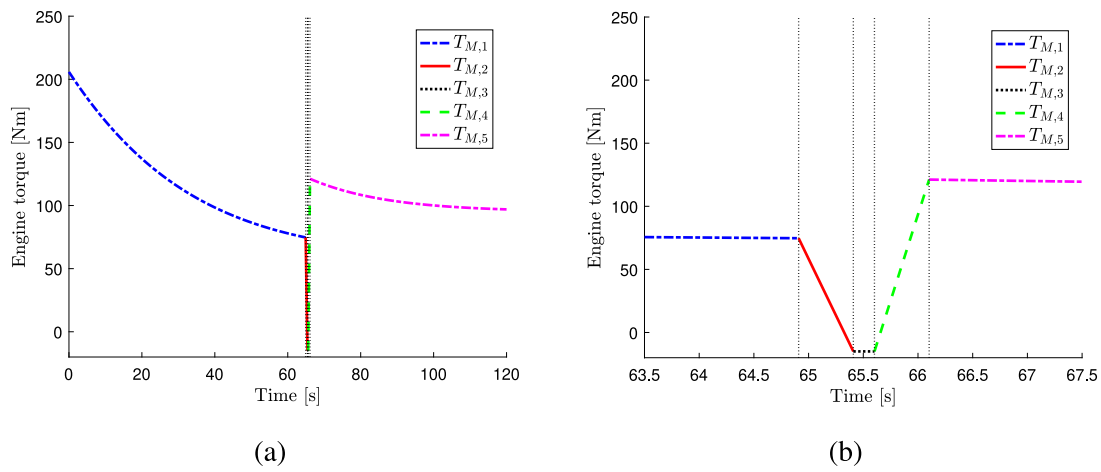**Fig. 10.** Input and output speeds (a), with a zoom during gearshift (b).

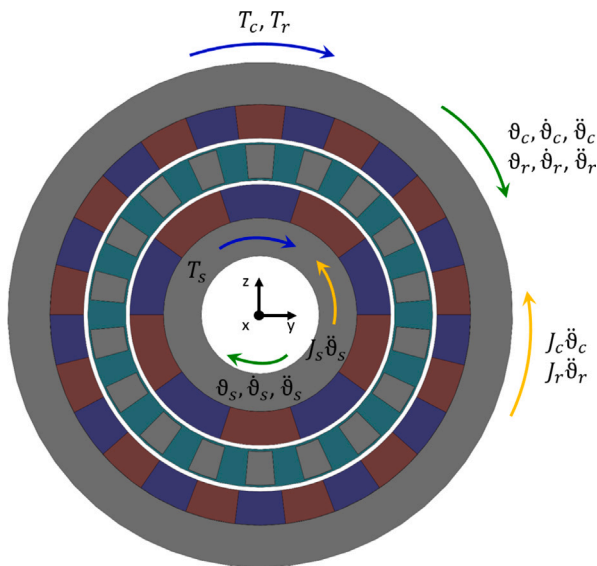**Fig. 11.** Motor torque in the five phases (a), with a zoom during gearshift (b).

Fig. 12. Free body diagram of a coaxial magnetic gear.

Magnetic torques and inertial effects of the three rotating elements are taken into account for writing the free body equilibrium. The

dynamic equations of the three rotors are reported in Eq. (16):

$$\begin{cases} J_r \ddot{\vartheta}_r = T_r - T_{MG_{cr}} \\ J_c \ddot{\vartheta}_c = T_c + T_{MG_{sc}} + T_{MG_{cr}} \\ J_s \ddot{\vartheta}_s = T_s - T_{MG_{sc}} \end{cases} \qquad (16)$$

where each rotor moment of inertia is represented by J, the external mechanical torques acting on the three rotors are indicated by T, while T_{MGsc} and T_{MGcr} are the internal magnetic torques, addressed to the magnetic flux in the airgaps between sun and carrier and between carrier and ring, respectively. Therefore, keeping the carrier fixed, T_s is the torque provided by the motor, if the sun is the power input, while T_r is the resistant torque on the output rotor, *i.e.* on the ring one. For the sake of clarity, dissipative terms such as bearing and seals torques, are not considered for the three rotors, since in the Simulink model bearing components are used inside the transmission, while magnetic losses inside the CMG are assumed negligible since an efficiency higher then 98.5% [26,56] is expected during steady state operation at fixed gear ratio, while losses may occur in the gearshift phase. The performance of a magnetic gear, in terms of transmissible torque, can be evaluated through the 2D FEM software FEMM [64] which, through a sequence of magneto-static solutions in a planar domain, is used to draw, mesh and compute the CMG magnetic properties. Dynamic effects related to induced eddy currents in conductive parts and losses in ferromagnetic materials are neglected [65]. On the other side, the nonlinear behaviour of the ferromagnetic materials is correctly considered due to the primary importance of this effect. In fact, flux magnetic saturation [66,67] is a critical aspect in thin yokes and in the flux modulator. Both these
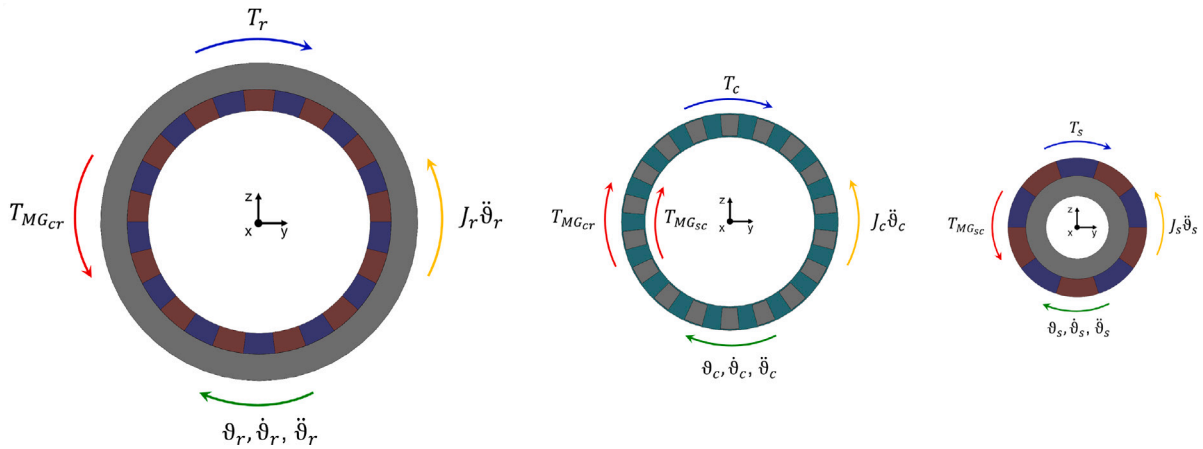
Fig. 13. FBDs of ring (left), carrier (centre) and sun (right) rotors of the CMG.
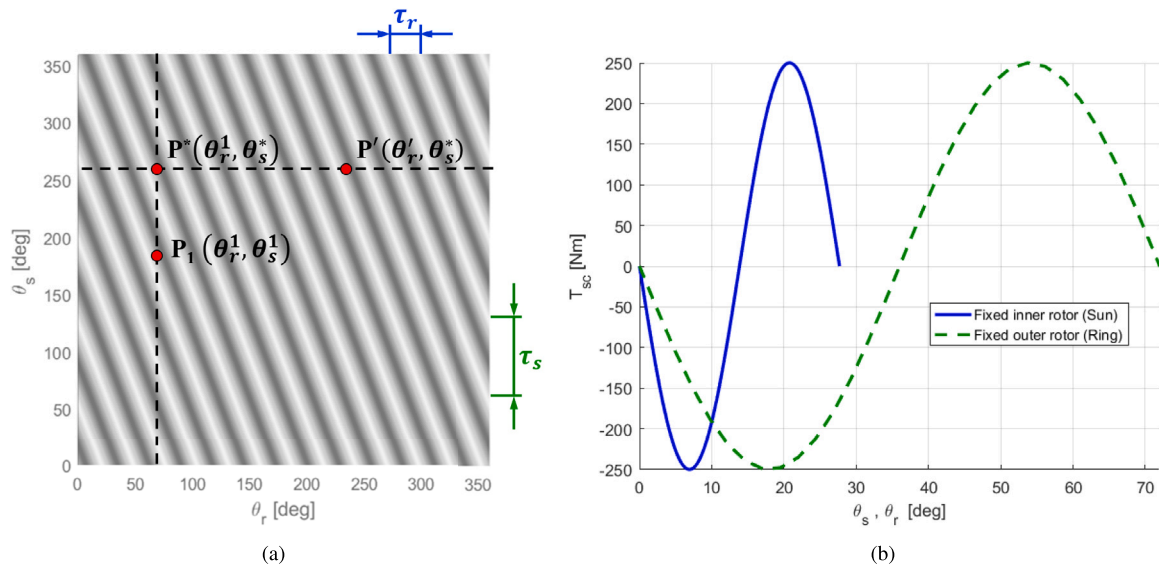

(a)

(b)

Fig. 14. Greyscale map of the CMG torque to highlight the periodicity along τ_s and τ_r (a), and same torque fixing the position of rotors one by one (b).

elements influence with their magnetic reluctance the magnetic flux generated by the PMs and thus reduce torque capability and efficiency of the device. The torque transmitted between the rotating elements of the CMG is computed using Maxwell's stress tensor, in the post-processing phase. The torque capability is evaluated in the two air-gaps between rotors, along different shell-paths with a final averaging of results [68]. For each different angular position, a FEM analysis is performed with the evaluation of the transmitted torque. The torque value depends on the angular relative position of rotors and hence its characteristic must be calculated for a sufficient number of angular positions, which well describe the torque trend. If the ferromagnetic poles are fixed, the torque is transmitted from the inner rotor to the outer rotor according to the torque map reported in Fig. 14(a). Each configuration, used to define the torque map, is identified by the two angles θ_s, and θ_r of sun and ring, respectively. The step discretisation of the two angles should be tiny enough to guarantee a good replicability of the map. The trend of torque map available at inner and outer rotor in simply scaled using the gear ratio value between sun and ring. These torque maps are characterised by sloped iso-torque lines. The slope of each curve at constant torque depends on the gear ratio of the magnetic gear between outer and inner rotor, and thus it depends on the number of permanent magnet poles on the two rotors according to Eq. (17). In

the considered CMG a gear ratio $\tau_{s/r} = -2.6$ is considered.

$$\tau_{s/r} = -\frac{N_r}{N_s} \tag{17}$$

As it is possible to notice from Fig. 14(a), the CMG periodicity can be analysed to reduce the number of FEM simulations necessary to evaluate the torque in any of the possible angular positions. Hence, it is possible to detect how each point at the same torque is repeated with a periodicity $\tau_s = 360°/N_S = 72°$ along the y axis of the figure, and a periodicity $\tau_r = 360°/N_R = 27.69°$ in the x axis. The torque is the same in the three points P_1, P' and P^*, which are highlighted in the figure, hence it is possible to replicate the entire map starting from one point and rotating the rotor with the highest number of PM poles in order to have the smaller interval for the periodicity. The torque trend along the periodicity, keeping fixed the ring or the sun rotors, is shown in Fig. 14(b). Moreover, when torque ripple is negligible, *i.e.* when a fractional gear ratio is chosen [10], only one FEM simulation, at the relative positions of the two rotors returning the maximum torque value $T_{MG_{max}}$, is necessary to replicate the torque map of Fig. 14(a), by using the sine function here reported:

$$T_{MG}\left(\theta_r, \theta_s\right) = -T_{MG_{max}} \sin\left(N_r\left(\theta_r - \frac{\theta_s}{\tau_{s/r}}\right) + \phi\right) \tag{18}$$
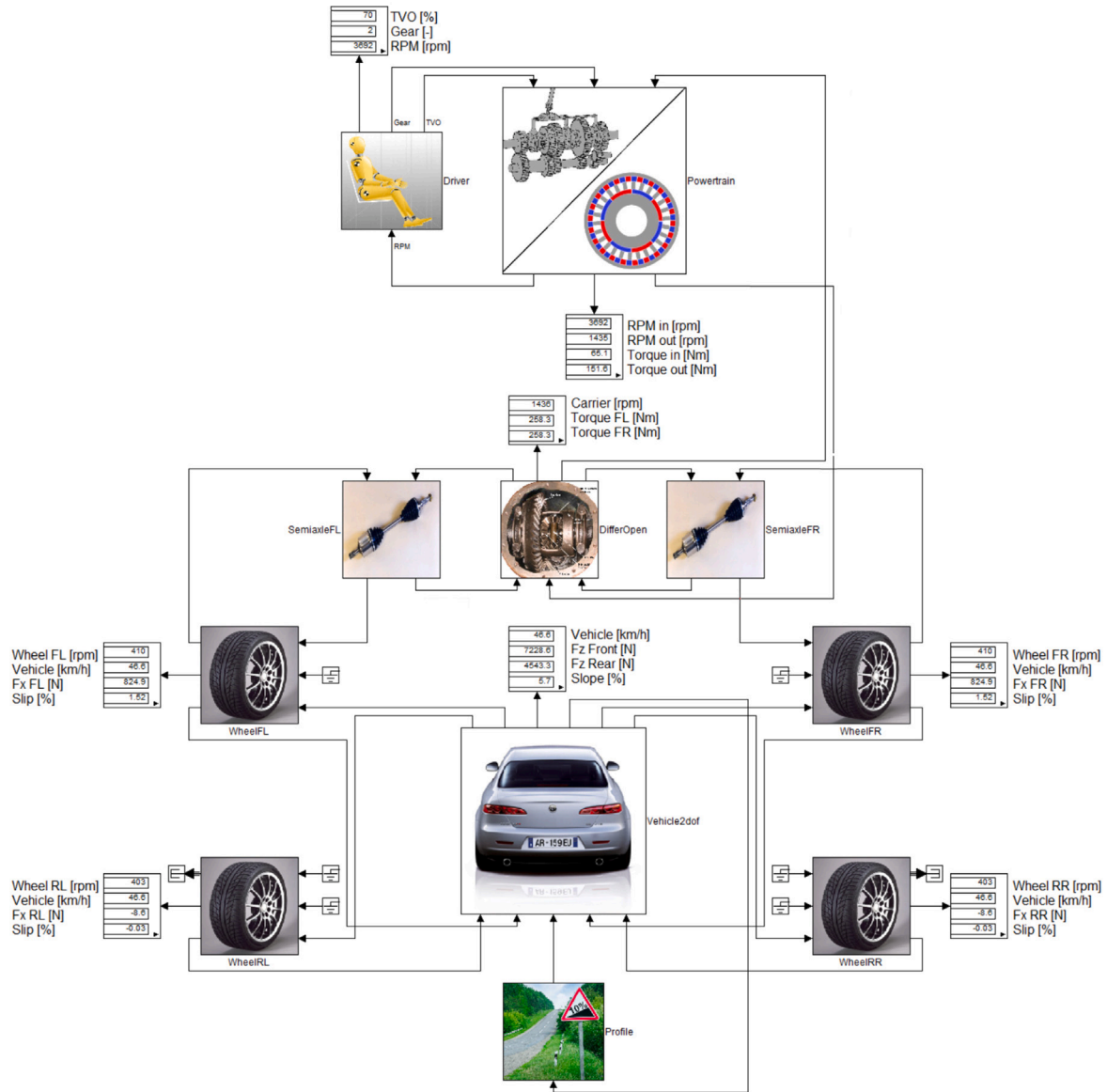
Fig. 15. Block-oriented vehicle driveline model.

where T_{MG} is the magnetic torque due to magnetic flux between two adjacent rotors, $T_{MG_{max}}$ is the maximum transmissible torque, $\theta_s = [0 : 360]°$ and $\theta_r = [0 : 360]°$ are the angular positions of sun and ring rotors, $\tau_{s/r}$ is defined in Eq. (17), N_R is the number of PM poles on ring rotor and ϕ is the sine phase computed using:

$$\phi = \arcsin\left(-\frac{\tilde{T}_{MG}}{T_{MG_{max}}}\right) - N_r\left(\theta_{r_0} - \frac{\theta_{s_0}}{\tau_{s/r}}\right) \tag{19}$$

where $\tilde{T}_{MG}$ is the torque evaluated at reference condition, corresponding to $\theta_{s_0} = \theta_{r_0} = 0°$.

5.3. Simulink model for gearshift

A model of the driveline, with a magnetic gearbox, based on the CMG transmission technology, is realised using the software Simulink, integrated in Matlab. The developed driveline model, shown in Fig. 15, is modelled with the block-oriented methodology [24,69,70]. Using this approach, the drivetrain is subdivided in its main components, from the driver to the wheels, and considers both dynamic and kinematic relationships. Moreover, this approach allows to highlight the correlation between each physical system and the corresponding model block, putting in evidence input/output component relations and interactions with global system behaviour and respect to other components.

A multi-sharing library of components is adopted to ensure a high feasibility level and to guarantee a user-friendly graphical interface. For each model component it is necessary to define the dynamic laws using the principle of mechanical equilibrium. The initial condition must be imposed, while constraints and possible dynamic constants must be defined. For each component, the input/output parameters are dependent from its own topology.

The above mentioned block-oriented approach is used to develop the Simulink model, shown in Fig. 15(a), which can be grouped in four main macro-blocks, i.e. driver, powertrain, differential, four wheels (2 driver and 2 driven) longitudinal vehicle model and road profile. The powertrain can include a magnetic transmission or a traditional one, as reported in the two possible layouts of Fig. 16(a) and (b), respectively. In the magnetic layout, an electric motor, modelled through an inertia block, which includes motor and input shaft inertia, is connected to
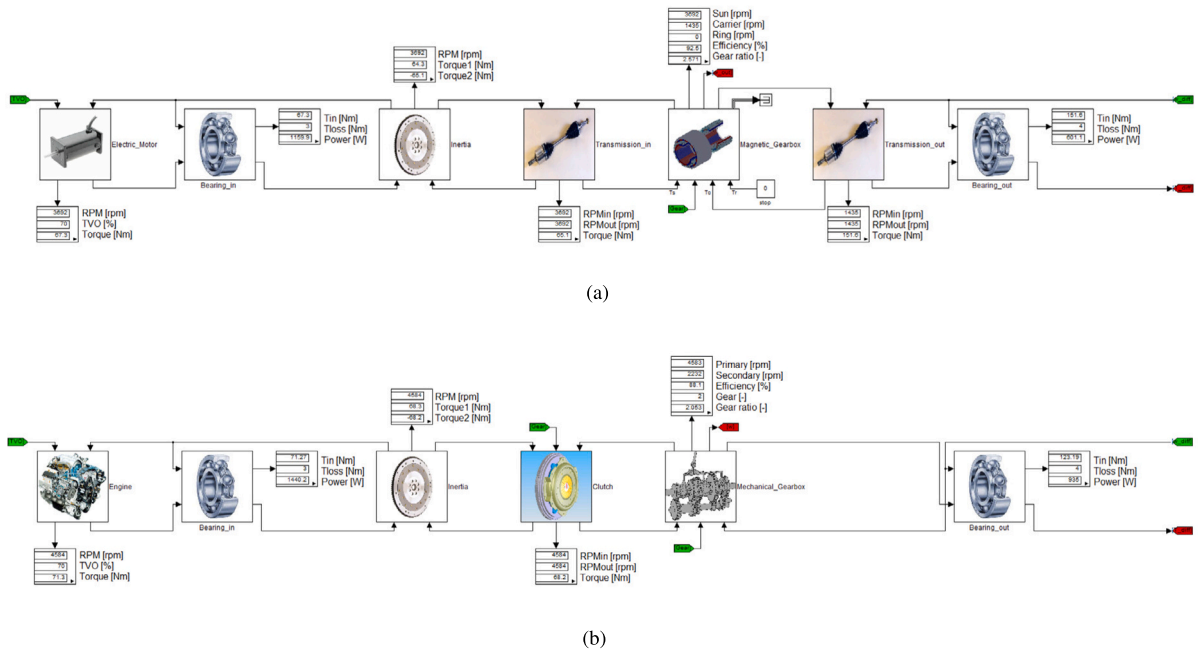
(a)

(b)

Fig. 16. Automotive driveline with magnetic transmission (a) or traditional powertrain (b) solutions.

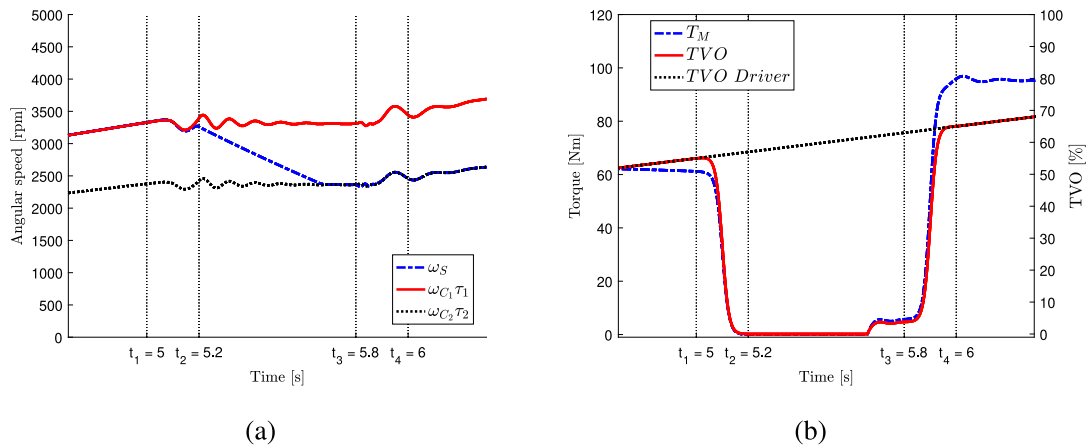(a)   (b)

Fig. 17. Speed (a) and torques with TVO (b) during simulated gearshift.

Table 2
Time parameters during gearshift.

Description	Parameter	Value
Starting time of gearshift	t_s	5 s
Time in neutral position	t_N	0.6 s
Time in control phase	t_C	0.6 s
Time for TVO modulation	t_{TVO}	0.2 s
Time to complete gearshift	t_{GS}	1 s
Starting time for disengaging	$t_1 = t_s$	5 s
Starting time of neutral position	$t_2 = t_1 + t_{TVO}$	5.2 s
Starting time of engaging	$t_3 = t_2 + t_N$	5.8 s
Gearshift completed at	$t_4 = t_3 + t_{TVO}$	6 s

the inner rotor (with inertia) of the magnetic gearbox, the outer rotor (ring) is rotationally kept fixed, since it can translate to ensure the gearshift, while the carrier of the magnetic gearbox (with inertia) is then connected to the differential crown, hence to vehicle and wheels. A magnetic gearbox with only two gear ratios has been considered in

the proposed model. This is a possible solution for EVs, while in case of ICE propulsion the number of gears should be increased. Alternatively, an internal combustion engine (ICE) could be used instead of the electric motor as input power source. In this case, the layout includes the clutch and the mechanical gearbox. A further possible layout could be a thermal power source directly connected to the magnetic gearbox, although it has not been considered for this research. Concerning the vehicle driver, he acts on the throttle valve opening (TVO), *i.e.* on the gas pedal, causing an acceleration or deceleration to the driveline, namely a transition phase, as function of the electric motor/ICE torque characteristic and the vehicle resistance load.

Inside the block magnetic gearbox the maps of maximum transmissible torque, as in Fig. 14(a), computed using FEMM at inner and carrier rotors for the different position of the two rotors, are used as a lookup table, after that the optimisation process was performed integrating FEMM into LUPOS software [71]. Four different maps are used, two for each transmission gear ratio. For sake of clarity, in each CMG the two torque maps are simply scaled by the transmission ratio, since the ripple is negligible. In the analysed simulation of the gearshift, the

magnetic gearbox is in neutral condition for a certain time. All the time parameters for gearshift are summarised in Table 2.

Additional details, in the complexity of the vehicle model, regards inertial terms, road-tyre interaction by means of the Pacejka '89 Magic formula [72,73], and aerodynamic and resistant effects.

A Proportional Integral Derivative (PID) controller is used to control the gearshift phase, in case of magnetic powertrain. Using this model, different gearshift conditions can be analysed, both in upshift and downshift, with a gearshift time comparable to that of high-performance mechanical gearboxes. According to values reported in Table 2, the controller is overlapped to the neutral condition of the magnetic gearbox. The axial movement of the external ring in the gearbox has been already depicted in Fig. 9 for the disengaging, neutral, and engaging conditions. The simulation results are presented in Fig. 17: during the gearshift, the rotational speeds of sun, *i.e.*, ω_S, and of carrier reported to the sun, according to the transmission gear ratios, *i.e.*, $\omega_{C_1}\tau_1$ and $\omega_{C_2}\tau_2$ are depicted in Fig. 17(a), while in Fig. 17(b) the motor torque T_M and the TVO are analysed. To avoid speed oscillations in the transmission driveline during the engaging phase, the TVO modulation between two different values must be properly managed, using a hyperbolic tangent trend instead of a linear increment/decrement, although a small oscillation is perceivable in Fig. 17(a).

The control logic acts on the TVO modulation during the gearshift, while the TVO during the operating conditions corresponds to the value imposed by the driver through the gas pedal, which in the time frame $4.5 \div 6.5$ s, reported in Fig. 17(b), has a constant increment from 50% to 70%. During the transition phase, TVO is modulated using a hyperbolic tangent from 55% to 0%, when the disengaging occurs, and then modulated from a certain value, equal to the transmission losses, up to 65% during the engaging phase. A PI controller is used, with a proportional gain K_P that is computed using:

$$K_P = \frac{T_M|_{(n_r\tau_2)}}{(n_s - n_r\tau_2)} \tag{20}$$

where $T_M|_{(n_r\tau_2)}$ is the torque that must be provided by the electric motor at the new rotational speed, depending on the transmission ratio τ_2, while $(n_s - n_r\tau_2)$ is the speed gap that must be filled with the use of proportional control during the gearshift phase, in this specific gearshift manoeuvre. Instead, the integral term was set at $K_I = 0.05K_P$.

6. Comments on prototype manufacturing

As already mentioned in Section 3, a magnetic gearbox prototype, with two transmission ratios, has been designed and built to validate the innovative technology, with dimensions and torques of a laboratory test bench. Different configurations, in terms of input/output power connections, can be tested. The proposed version, depicted in Fig. 18(a), consists of a structure, which includes the rotors of the CMG, input/output shafts and all the bearing used for switching the configurations:

- on the top side the carrier is connected to the red shaft through an element of connection, *e.g.* a flange, while the ring with PMs is fixed to the middle brown plate;
- on the bottom side, the carrier is fixed to the same brown plate and the ring rotates at the same speed of the red shaft.

Furthermore, a conical coupling is adopted for the connection of the green shaft, which is assumed as the input shaft of the prototype, with the inner rotor (sun) of the active CMG. In this way, it is possible to avoid the unwanted issue of dynamic unbalance due to a coupling with parallel keys. With this configuration, a speed reducer/torque multiplier is achieved, although a speed multiplier/torque reducer can be realised just switching input/output shafts.

The axial translation of the carrier inside the gearbox is guaranteed by the gearshift mechanism illustrated in Fig. 18(b). It is composed
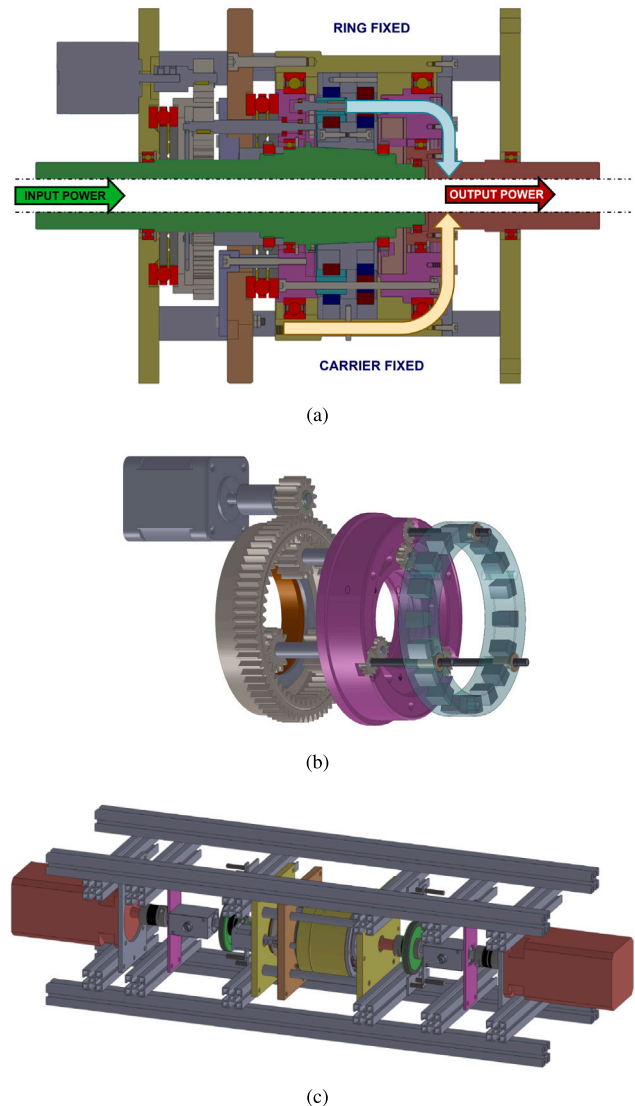

(a)

(b)

(c)

Fig. 18. CAD model of magnetic gearbox prototype (a), with gearshift mechanism (b) and its test bench (c).

by a step motor, connected to a mechanical gear, which is externally engaged with a ring gear. Then three planets are used to put in rotation three pins which are connected on the other side with three screws by means of another mechanical coupling. All these gears are realised in Delrin material. Finally the rotary motion of the screws is converted into a translational motion by means of three threaded bushing, inserted in the carrier.

The proposed prototype has the advantage to be completely independent from its test bench structure, realised in a modular solution with Bosh profiles, as reported in Fig. 18(c). This aspect guarantees a higher facility in mounting and dismounting procedures. The test bench structure is completely symmetric with respect to the magnetic gearbox and one side of the transmission driveline, which includes: a first elastic joint, a magnetic incremental encoder, a torque sensor, another elastic joint, and a brushless motor. Two electric motors are chosen for the proposed solution; the driver can control them either through a torque loop or velocity loop, as done in [74] to analyse the torsional dynamic performance of a mechanical transmission, allowing the testing of the several working conditions previously described. Other details on the driveline components are listed in [28].

As regards the constructive choices for the magnetic gearbox prototype, PMs of inner and outer rotors have been segmented to increase
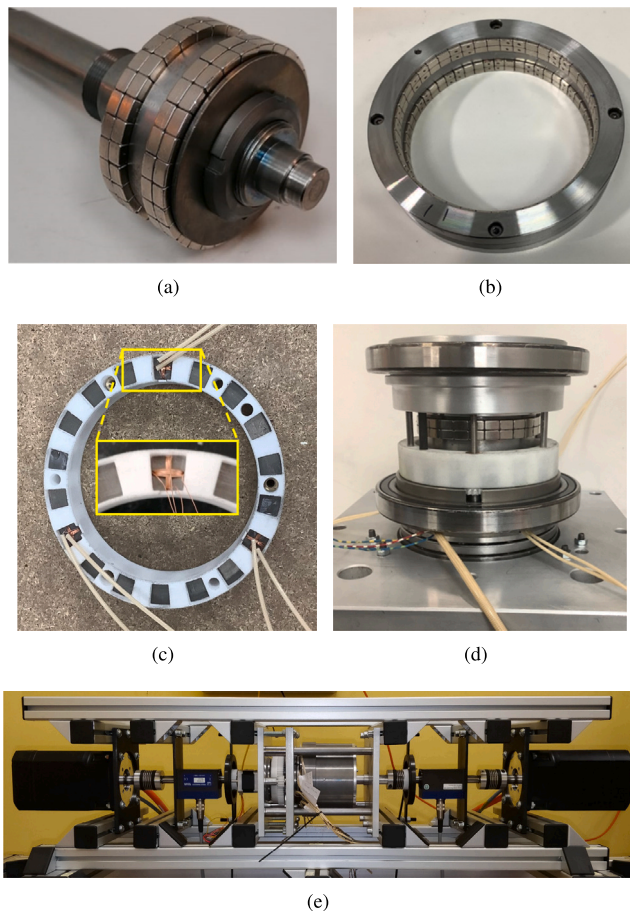
Fig. 19. Assembled sun (a) and ring (b) rotors, carrier (c) with ferromagnetic poles, inner of magnetic gearbox prototype (d) during mounting and assembled test rig (e).

the magnetic transmission efficiency. As stated in [26], the main effect of PMs segmentation consists in the reduction of the equivalent PMs conductivity leading to lower eddy current losses in PMs. This is usually achieved with segmentation in both circumferential and axial direction. It has been highlighted that the effect of PMs segmentation is higher at the outer rotor, where the eddy current is equally distributed in the segments, while at the inner rotor PMs the eddy currents distribution locally concentrates near the airgaps. The inner (Fig. 19(a)) and outer (Fig. 19(b)) rotors of the magnetic gearbox have been assembled after gluing the segmented PMs on the corresponding inner and outer yokes. In Fig. 19(c), the carrier, holding the ferromagnetic poles, is depicted. Radial and tangential coils have been realised on three of the ferromagnetic poles to measure the magnetic flux inside the gearbox, using the Faraday law. Preliminary experimental results have already been presented in [28], analysing the effect of different rotational speeds and loads on the magnetic flux. Finally, in Fig. 19(d) the magnetic gearbox is assembled and then mounted on the test bench (Fig. 19(e)). The test bench will be used for a future characterisation of losses inside the transmission, splitting the two contributions of bearing losses and magnetic losses. Also, gearshift tests will be performed after implementing the gearshift procedure in the test bench controller.

7. Conclusions

In this paper, the innovative industrial technology of magnetic gearbox is proposed as potential alternative to conventional mechanical gearboxes, characterised by a series of issues as noise and vibrations.

Four main topologies, based on a different translating element, have been suggested and patented, and one of them has been prototyped, for technology validation and characterisation of the magneto-mechanical properties. A Matlab-Simulink model has been developed for the control of transition phase, obtaining results in agreement with the analytical approach previously presented. Preliminary results has proven to achieve high levels of efficiency of the technology, both as torque multiplier and speed multiplier. A future continuation of this work will focus on the implementation of the magnetic gearbox control strategies together with the full operation of the prototype with time-comparable vehicle manoeuvres of upshift and downshifts. Meanwhile, another possible future extension of this work could be a deeper investigation of electromagnetic phenomena during the gearshift procedure, through a time-domain analysis in a multiphysics 3D software for magneto-mechanical problems.

Declaration of competing interest

The authors declare that they have no known competing financial interests or personal relationships that could have appeared to influence the work reported in this paper.

References

[1] M. Sharifzadeh, M. Pisaturo, A. Senatore, Real-time identification of dry-clutch frictional torque in automated transmissions at launch condition, Proc. Inst. Mech. Eng. D 234 (2–3) (2020) 586–598, http://dx.doi.org/10.1177/0954407019857268.

[2] Y. Wang, M. Filippini, N. Bianchi, P. Alotto, A review on magnetic gears: Topologies, computational models, and design aspects, IEEE Trans. Ind. Appl. 55 (2019) 4557–4566, http://dx.doi.org/10.1109/TIA.2019.2916765.

[3] P.M. Tlali, R.J. Wang, S. Gerber, Magnetic gear technologies: A review, in: 2014 International Conference on Electrical Machines (ICEM), IEEE, 2014, pp. 544–550, http://dx.doi.org/10.1109/ICELMACH.2014.6960233.

[4] E. Gouda, S. Mezani, L. Baghli, A. Rezzoug, Comparative study between mechanical and magnetic planetary gears, IEEE Trans. Magn. 47 (2011) 439–450, http://dx.doi.org/10.1109/TMAG.2010.2090890.

[5] M. Desvaux, B. Multon, H.B. Ahmed, S. Sire, Behaviour comparison between mechanical epicyclic gears and magnetic gears, in: International Symposium on Multibody Systems and Mechatronics, Mechanisms and Machine Science, Springer, 2017, pp. 401–410, http://dx.doi.org/10.1007/978-3-319-67567-1_38.

[6] G. Duan, T. Gupta, E. Sutton, M. Wang, M.C. Gardner, S.A. Khan, B. Praslicka, Cycloidal magnetic gear combining axial and radial topologies, IEEE Trans. Energy Convers. 37 (3) (2022) 2130–2137, http://dx.doi.org/10.1109/TEC.2022.3171105.

[7] V. Mateev, M. Todorova, I. Marinova, Design aspects of conical coaxial magnetic gears, Energies 16 (10) (2023) 4191, http://dx.doi.org/10.3390/en16104191.

[8] G. Ruiz-Ponce, M.A. Arjona, C. Hernandez, R. Escarela-Perez, A review of magnetic gear technologies used in mechanical power transmission, Energies 16 (4) (2023) 1721, http://dx.doi.org/10.3390/en16041721.

[9] K. Atallah, D. Howe, A novel high-performance magnetic gear, IEEE Trans. Magn. 37 (2001) 2844–2846, http://dx.doi.org/10.1109/20.951324.

[10] K. Atallah, S.D. Calverley, D. Howe, Design, analysis and realisation of a high-performance magnetic gear, IEE Proc.-Electr. Power Appl. 151 (2004) 135–143.

[11] L. Jing, W. Tang, T. Wang, T. Ben, R. Qu, Performance analysis of magnetically geared permanent magnet brushless motor for hybrid electric vehicles, IEEE Trans. Transp. Electrif. 8 (2) (2022) 2874–2883, http://dx.doi.org/10.1109/TTE.2022.3151681.

[12] D. Fodorean, M.A. Fakhfakh, State of the art of magnetic gears their design and characteristics with respect to EV application, in: Modeling and Simulation for Electric Vehicle Applications, Chapter 4, InTech, 2016, pp. 73–95.

[13] K. Atallah, J. Wang, S.D. Calverley, S. Duggan, Design and operation of a magnetic continuously variable transmission, IEEE Trans. Ind. Appl. 48 (2012) 1288–1295, http://dx.doi.org/10.1109/TIA.2012.2199451.

[14] G. Tavakoli, A. Jabbari, M.R. Sheykholeslami, A semi-analytical, numerical and experimental study on performance characteristics of a novel hybrid-rotor CVT magnetic gearbox, Proc. Inst. Mech. Eng. D (2022) 1–12, http://dx.doi.org/10.1177/09544070221103162.

[15] Y. Mao, S. Niu, Y. Yang, Differential evolution-based multiobjective optimization of the electrical continuously variable transmission system, IEEE Trans. Ind. Electron. 65 (2018) 2080–2089, http://dx.doi.org/10.1109/TIE.2017.2733458.

[16] V. Mucino, Z. Lu, J. Smith, M. Kimcikiewicz, B. Cowan, Design of continuously variable power split transmission systems for automotive applications, Proc. Inst. Mech. Eng. D 215 (4) (2001) 469–478, http://dx.doi.org/10.1243/0954407011528086.

[17] A. Abdel-Khalik, S. Ahmed, A. Massoud, A bearingless coaxial magnetic gearbox, Alex. Eng. J. 53 (3) (2014) 573–582, http://dx.doi.org/10.1016/j.aej.2014.06.002.

[18] E. Bonisoli, S. Venturini, S. Cavallaro, Nonlinear characterisation of a rotor on passive magnetic supports, Int. J. Mech. Control 23 (1) (2022) 121–128.

[19] Y. Mao, Y. Yang, Optimization of magnetic gear patterns based on taguchi method combined with genetic algorithm, Energies 15 (14) (2022) 4963, http://dx.doi.org/10.3390/en15144963.

[20] L. Jing, W. Liu, W. Tang, R. Qu, Design and optimization of coaxial magnetic gear with double-layer pms and spoke structure for tidal power generation, IEEE/ASME Trans. Mechatronics (2023) http://dx.doi.org/10.1109/TMECH.2023.3261987.

[21] X. Zhang, X. Liu, Z. Chen, A novel dual-flux-modulator coaxial magnetic gear for high torque capability, IEEE Trans. Energy Convers. 33 (2) (2017) 682–691, http://dx.doi.org/10.1109/TEC.2017.2778285.

[22] G. Jungmayr, J. Loeffler, B. Winter, F. Jeske, W. Amrhein, Magnetic gear: Radial force, cogging torque, skewing, and optimization, IEEE Trans. Ind. Appl. 52 (5) (2016) 3822–3830, http://dx.doi.org/10.1109/ECCE.2015.7309783.

[23] M. Desvaux, B. Multon, S. Sire, H.B. Ahmed, Analytical iron loss model for the optimization of magnetic gear, in: 2017 IEEE International Electric Machines and Drives Conference (IEMDC), IEEE, 2017, pp. 1–8, http://dx.doi.org/10.1109/IEMDC.2017.8002255.

[24] M. Velardocchia, E. Bonisoli, E. Galvagno, A. Vigliani, A. Sorniotti, Efficiency of epicyclic gears in automated manual transmission systems, in: In 8th International Conference on Engines for Automobiles, SAE Technical Paper, 2007, http://dx.doi.org/10.4271/2007-24-0139.

[25] V. Cirimele, L. Dimauro, M. Repetto, E. Bonisoli, Multi-objective optimisation of a magnetic gear for powertrain applications, Int. J. Appl. Electromagn. Mech. 60 (2019) S25–S34, http://dx.doi.org/10.3233/JAE-191103.

[26] M. Filippini, P. Alotto, V. Cirimele, M. Repetto, C. Ragusa, L. Dimauro, E. Bonisoli, Magnetic loss analysis in coaxial magnetic gears, Electronics (Switzerland) 8 (2019) http://dx.doi.org/10.3390/electronics8111320.

[27] E. Bonisoli, L. Dimauro, A. Vigliani, M. Velardocchia, M. Repetto, V. Cirimele, P. Alotto, M. Filippini, Patent: Magnetic gearshift system, WO 2022/013774 A1, 2020-2022, pp. 1–46.

[28] P. Alotto, E. Armando, E. Bonisoli, V. Cirimele, L. Dimauro, M. Filippini, M. Repetto, P. Squillari, R. Torchio, M. Velardocchia, Design, analysis and realisation of a magnetic gear prototype with experimental validation, in: 2022 23rd International Conference on the Computation of Electromagnetic Fields (COMPUMAG), IEEE, 2022, pp. 1–4, http://dx.doi.org/10.1109/COMPUMAG55718.2022.9827514.

[29] L. Dimauro, E. Bonisoli, M. Repetto, Dynamic behaviour and magneto-mechanical efficiency of a contactless magnetic transmission, in: Rotating Machinery, Optical Methods & Scanning LDV Methods, Volume 6, Springer, 2023, pp. 129–138, http://dx.doi.org/10.1007/978-3-031-04098-6_14.

[30] M. Filippini, P. Alotto, M. Repetto, E. Bonisoli, V. Cirimele, Patent: Differential and vehicle comprising such differential, IT 2018/00010648 A1–WO 2020/110064 A1, 2018-2020.

[31] H.W. Müller, Epicyclic Drive Trains: Analysis, Synthesis, and Applications, Wayne State University Press, 1982.

[32] S. Pakdelian, N.W. Frank, H.A. Toliyat, Damper windings for the magnetic gear, in: 2011 IEEE Energy Conversion Congress and Exposition, IEEE, 2011, pp. 3974–3981, http://dx.doi.org/10.1109/ECCE.2011.6064310.

[33] A. Castellano, M. Cammalleri, Power losses minimization for optimal operating maps in power-split HEVs: a case study on the Chevrolet Volt, Appl. Sci. 11 (17) (2021) 7779, http://dx.doi.org/10.3390/app11177779.

[34] A. Tota, E. Galvagno, L. Dimauro, A. Vigliani, M. Velardocchia, Energy management strategy for hybrid multimode powertrains: Influence of inertial properties and road inclination, Appl. Sci. 11 (24) (2021) 11752, http://dx.doi.org/10.3390/app112411752.

[35] E. Galvagno, A. Vigliani, M. Velardocchia, Transient response and frequency domain analysis of an electrically variable transmission, Adv. Mech. Eng. 10 (5) (2018) 1–12, http://dx.doi.org/10.1177/1687814018776182.

[36] S. Cho, K. Ahn, J.M. Lee, Efficiency of the planetary gear hybrid powertrain, Proc. Inst. Mech. Eng. D 220 (10) (2006) 1445–1454, http://dx.doi.org/10.1243/09544070JAUTO176.

[37] Q. Sun, W. Wu, Z. Peng, W. Xing, H. Wang, A rapid approximate dynamic programing based on constraint satisfaction for a series-parallel hybrid electric vehicle with a three-speed gearbox, Proc. Inst. Mech. Eng. D (2022) 1–15, http://dx.doi.org/10.1177/09544070221105399.

[38] P. Dong, Y. Wang, S. Zhao, Z. Gao, Y. Zhao, Y. Cao, P. Zhang, Design and experimental study of novel multi-stage gearbox, Proc. Inst. Mech. Eng. D 235 (1) (2021) 105–113, http://dx.doi.org/10.1177/0954407020945823.

[39] C.C. Huang, M.C. Tsai, D.G. Dorrell, B.J. Lin, Development of a magnetic planetary gearbox, IEEE Trans. Magn. 44 (2008) 403–412, http://dx.doi.org/10.1109/TMAG.2007.914665.

[40] X. Liu, K.T. Chau, J.Z. Jiang, C. Yu, Design and analysis of interior-magnet outer-rotor concentric magnetic gears, J. Appl. Phys. 105 (2009) 07F101, http://dx.doi.org/10.1063/1.3058619.

[41] S. Gerber, R.J. Wang, Evaluation of a prototype magnetic gear, in: Proceedings of the IEEE International Conference on Industrial Technology, 2013, pp. 319–324, http://dx.doi.org/10.1109/ICIT.2013.6505692.

[42] K. Uppalapati, J. Kadel, J. Wright, K. Li, W. Williams, J.Z. Bird, A low assembly cost coaxial magnetic gearbox, in: 2016 IEEE 2nd Annual Southern Power Electronics Conference (SPEC), IEEE, 2016, pp. 1–6, http://dx.doi.org/10.1109/SPEC.2016.7846207.

[43] C.G.C. Neves, M.F. Goettems, A.F.F. Filho, Construction of a coaxial magnetic gear, in: 18th International Symposium on Electromagnetic Fields in Mechatronics, Electrical and Electronic Engineering, 2017, pp. 2–5.

[44] E. Galvagno, G.R. Guercioni, A. Vigliani, Sensitivity analysis of the design parameters of a dual-clutch transmission focused on NVH performance, SAE Technical Paper, 2016-01-1127, 2016, pp. 1–12, http://dx.doi.org/10.4271/2016-01-1127.

[45] E. Galvagno, A. Tota, M. Velardocchia, A. Vigliani, Enhancing transmission NVH performance through powertrain control integration with active braking system, SAE Technical Paper, 2017-01-1778, 2017, pp. 1–6, http://dx.doi.org/10.4271/2017-01-1778.

[46] E. Galvagno, L. Dimauro, G. Mari, M. Velardocchia, A. Vella, Dual clutch transmission vibrations during gear shift: A simulation-based approach for clunking noise assessment, SAE Technical Paper, 2019-01-1553, June, 2019, pp. 1–12, http://dx.doi.org/10.4271/2019-01-1553.

[47] G.R. Guercioni, E. Galvagno, A. Tota, A. Vigliani, T. Zhao, Driveline backlash and half-shaft torque estimation for electric powertrains control, SAE Technical Paper, 2018-01-1345, 2018, pp. 1–9, http://dx.doi.org/10.4271/2018-01-1345.

[48] A. Hajnayeb, J.S. Fernando, Q. Sun, Effects of vehicle driveline parameters and clutch judder on gearbox vibrations, Proc. Inst. Mech. Eng. D 236 (1) (2022) 84–98, http://dx.doi.org/10.1177/09544070211015939.

[49] R. Brancati, E. Rocca, S. Savino, F. Timpone, Experimental analysis of the relative motion of a gear pair under rattle conditions induced by multi-harmonic excitation, in: Proceedings of the World Congress on Engineering, Vol. 2, 2015, pp. 1–3.

[50] E. Bonisoli, C. Rosso, S. Venturini, D. Rovarino, M. Velardocchia, Improvements on design and validation of automotive steel wheels, in: Advances in Mechanism and Machine Science: Proceedings of the 15th IFToMM World Congress on Mechanism and Machine Science 15, Springer, 2019, pp. 1639–1649, http://dx.doi.org/10.1007/978-3-030-20131-9_162.

[51] D. Rovarino, L.A. Comino, E. Bonisoli, C. Rosso, S. Venturini, M. Baecker, A. Gallrein, Hardware and virtual test-rigs for automotive steel wheels design, SAE Technical Paper, 2020-01-1231, April, 2020, pp. 1–9, http://dx.doi.org/10.4271/2020-01-1231.

[52] N. Niguchi, K. Hirata, A. Zaini, Electromagnetic vibration analysis and measurement of a magnetic gear, IEEJ J. Ind. Appl. 2 (6) (2013) 261–268, http://dx.doi.org/10.1541/ieejjia.2.261.

[53] J.Y. Lee, J.H. Chang, Vibration and noise characteristics of coaxial magnetic gear according to low-speed rotor structure, J. Mech. Sci. Technol. 31 (2017) 2723–2728, http://dx.doi.org/10.1007/s12206-017-0515-4.

[54] S.S. Nielsen, H.Y. Wong, H. Baninajar, J.Z. Bird, P.O. Rasmussen, Pole and segment combination in concentric magnetic gears: Vibrations and acoustic signature, IEEE Trans. Energy Convers. 37 (3) (2022) 1644–1654, http://dx.doi.org/10.1109/TEC.2022.3151654.

[55] S. Jo, H. Shin, J. Chang, Dynamic analysis of surface-mounted permanent magnet type coaxial magnetic gear with damper bar considering magnetic field modulation effect, IEEE Access 10 (2022) 33616–33627, http://dx.doi.org/10.1109/ACCESS.2022.3161633.

[56] M. Filippini, R. Torchio, P. Alotto, E. Bonisoli, L. Dimauro, M. Repetto, A new class of devices: Magnetic gear differentials for vehicle drivetrains, IEEE Trans. Transp. Electrif. 9 (2) (2023) 2382–2397, http://dx.doi.org/10.1109/TTE.2022.3208628.

[57] L. Jian, K.T. Chau, J.Z. Jiang, An integrated magnetic-geared permanent-magnet in-wheel motor drive for electric vehicles, in: 2008 IEEE Vehicle Power and Propulsion Conference, IEEE, 2008, pp. 1–6, http://dx.doi.org/10.1109/VPPC.2008.4677512.

[58] G. De Filippis, B. Lenzo, A. Sorniotti, P. Gruber, W. De Nijs, Energy-efficient torque-vectoring control of electric vehicles with multiple drivetrains, IEEE Trans. Veh. Technol. 67 (6) (2018) 4702–4715, http://dx.doi.org/10.1109/TVT.2018.2808186.

[59] A. Moghimi, M. Hosseini Aliabadi, H. Feshki Farahani, Triple-speed coaxial magnetic gear for wind turbine applications: Introduction and comprehensive analysis, COMPEL-The Int. J. Comput. Math. Electr. Electron. Eng. 41 (4) (2022) 1223–1244, http://dx.doi.org/10.1108/COMPEL-01-2022-0001.

[60] X. Qi, Y. Yang, X. Wang, Z. Zhu, Analysis and optimization of the gear-shifting process for automated manual transmissions in electric vehicles, Proc. Inst. Mech. Eng. D 231 (13) (2017) 1751–1765, http://dx.doi.org/10.1177/0954407016685461.

[61] G. Min, H. Son, M. Song, S. Hong, M. Kim, Y. Choi, H. Kim, Development of a gear fork control algorithm to improve the shift quality of a dual-clutch transmission, Proc. Inst. Mech. Eng. D 230 (11) (2016) 1477–1487, http://dx.doi.org/10.1177/0954407015613266.

[62] Drivetrain losses (efficiency), (Date accessed 21/12/2022) URL https://x-engineer.org/drivetrain-losses-efficiency/.

[63] P. Baldissera, Proposal of a coast-down model including speed-dependent coefficients for the retarding forces, Proc. Inst. Mech. Eng. P 231 (2) (2017) 154–163, http://dx.doi.org/10.1177/1754337116658587.

[64] D. Meeker, Finite Element Method Magnetics, (Date accessed 28/11/2022) URL https://www.femm.info/wiki/HomePage.

[65] M. Filippini, P. Alotto, An optimization tool for coaxial magnetic gears, COMPEL-Int. J. Comput. Math. Electr. Electron. Eng. 36 (2017) 1526–1539, http://dx.doi.org/10.1108/COMPEL-02-2017-0068.

[66] L. Alberti, E. Fornasiero, N. Bianchi, Impact of the rotor yoke geometry on rotor losses in permanent-magnet machines, IEEE Trans. Ind. Appl. 48 (1) (2011) 98–105, http://dx.doi.org/10.1109/ECCE.2010.5618299.

[67] S. Gerber, R. Wang, Analysis of the end-effects in magnetic gears and magnetically geared machines, in: 2014 International Conference on Electrical Machines (ICEM), IEEE, 2014, pp. 396–402, http://dx.doi.org/10.1109/ICELMACH.2014.6960211.

[68] F. Henrotte, G. Deliége, K. Hameyer, The eggshell method for the computation of electromagnetic forces on rigid bodies in 2D and 3D, in: CEFC 2002, 2002, pp. 16–18.

[69] M. Velardocchia, N. D'Alfio, E. Bonisoli, E. Galvagno, F. Amisano, A. Sorniotti, Block-oriented models of torque gap filler devices for AMT transmissions, SAE Technical Paper, 2008-01-0631, 2008, pp. 1–12, http://dx.doi.org/10.4271/2008-01-0631.

[70] L. Dimauro, A. Tota, E. Galvagno, M. Velardocchia, Torque allocation of hybrid electric trucks for drivability and transient emissions reduction, Appl. Sci. 13 (6) (2023) 3704, http://dx.doi.org/10.3390/app13063704.

[71] E. Bonisoli, L. Dimauro, S. Venturini, Lupos: open-source scientific computing in structural dynamics, in: Proceedings of the 41st IMAC, a Conference and Exposition on Structural Dynamics, Springer, Austin, Texax, USA, 2023.

[72] H.B. Pacejka, E. Bakker, The magic formula tyre model, Veh. Syst. Dyn. 21 (S1) (1992) 1–18.

[73] H.B. Pacejka, Tyre and Vehicle Dynamics, Elsevier, 2005.

[74] E. Galvagno, M. Velardocchia, A. Tota, L. Zerbato, A.D. Vella, Torsional dynamic performance of a transmission test bench: An investigation on the effect of motors controllers parameters, in: Proceedings of I4SDG Workshop 2023, Springer Nature Switzerland, 2023, pp. 441–447, http://dx.doi.org/10.1007/978-3-031-32439-0_50.